Cerebral Cortex January 2014;24:1–16
doi:10.1093/cercor/bhs208
Advance Access publication September 25, 2012

Quantification of Early Stages of Cortical Reorganization of the Topographic Map of V1 Following Retinal Lesions in Monkeys

Elia P. Botelho[1,2], Cecília Ceriatte[1], Juliana G.M. Soares[1], Ricardo Gattass[1] and Mario Fiorani[1]

[1]Programa de Neurobiologia, Universidade Federal do Rio de Janeiro, Instituto de Biofísica Carlos Chagas Filho, Rio de Janeiro, RJ 21941-900, Brazil and [2]Current address: University of California, Los Angeles, SEMEL Institute 58-241, Los Angeles, CA 90024, USA

Address correspondence to Mario Fiorani, Laboratório de Neurobiologia, Instituto de Biofísica Carlos Chagas Filho, CCS, Bloco G, Sala G2-09, Cidade Universitária, Rio de Janeiro, RJ 21941-900, Brazil. Email: mfiorani@biof.ufrj.br

We quantified the capacity for reorganization of the topographic representation of area V1 in adult monkeys. Bias-free automated mapping methods were used to delineate receptive fields (RFs) of an array of neuronal clusters prior to, and up to 6 h following retinal lesions. Monocular lesions caused a significant reorganization of the topographic map in this area, both inside and outside the cortical lesion projection zone (LPZ). Small flashed stimuli revealed responses up to 0.85 mm inside the boundaries of the LPZ, with RFs representing regions of undamaged retina immediately surrounding the lesion. In contrast, long moving bars that spanned the scotoma resulting from the lesion revealed responsive units up to 1.87 mm inside the LPZ, with RFs representing interpolated responses in this region. This reorganization is present immediately after monocular retinal lesioning. Both stimuli showed a similar and significant (5-fold) increase of the RF scatter in the LPZ, 0.56 mm (median), compared with the undamaged retina, 0.12 mm. Our results reveal an array of preexisting subthreshold functional connections of up to 2 mm in V1, which can be rapidly mobilized independently from the differential qualitative reorganization elicited by each stimulus.

Keywords: cortical reorganization, electrophysiological recordings, intrinsic connections, primary visual cortex, primate

Introduction

The topographic reorganization of the adult primary visual cortex (area V1) following retinal lesions has been the subject of several studies with conflicting results. Cortical map reorganization at the retinal lesion projection zones (LPZ) in V1 following monocular or binocular lesions has been reported in some studies (Heinen and Skavenski 1991; Gilbert and Wiesel 1992; Chino et al. 1995; Darian-Smith and Gilbert 1995; Schmid et al. 1995, 1996; Calford et al. 1999, 2000; Waleszczyk et al. 2003; Giannikopoulos and Eysel 2006), but not in others (Murakami et al. 1997; Smirnakis et al. 2005). Some of the studies that showed plasticity indicated that reorganization after monocular lesion only became manifest after removal of the opposite (nontreated) eye (Kaas et al. 1990; Chino et al. 1992).

Throughout the studies providing evidence for V1 reorganization, controversy exists regarding the temporal and spatial extents of this reorganization (Heinen and Skavenski 1991; Chino et al. 1992; Gilbert and Wiesel 1992; Darian-Smith and Gilbert 1995; Calford et al. 1999). An important question for understanding the temporal and spatial aspects of reorganization is whether the changes are caused by alterations in the properties of pre-existing synaptic connections or by the rewiring of cortical circuits. Another issue is related to the type of stimulus used. Different stimuli can lead to different estimates of the extent of reorganization, inasmuch as those stimuli can recruit different neural circuitry (Angelucci et al. 2002). In this context, Fiorani et al. (1992) showed that throughout V1, cells were capable of responding to long moving bars presented outside the classical RF location, showing that the cortical circuits can interpolate the stimulus position based on the stimulation of adjacent retinal areas. For example, a long bar that spanned the width of an overlying mask or of a naturally occurring blind spot could still elicit an excitatory response in the correct topographic location, provided that the stimulus configuration suggested continuity across the gap. Other researchers have also observed a nontopographic filling-in capability in studies using other types of large (nontopographic) stimuli (Pettet and Gilbert 1992; Volchan and Gilbert 1995; Komatsu et al. 2000).

We designed the present study with 2 different fully automated RF mapping procedures, to access the contributions of short- and long-range mechanisms in the topographic reorganization of V1 in the hours following retinal lesioning. In addition to small flashed visual stimuli to probe the short-range RF reorganization (presumably due only to unmasking of pre-existing feedforward afferents), we also used long moving bars to probe the long-range RF reorganization that could be attributed to horizontal or feedback mechanisms. These stimulation methods are referred to throughout the paper as "local" and "global" mappings, respectively. In addition to examining the extent to which cells inside the LPZ are connected through intrinsic horizontal and feedback connections (Angelucci and Bressloff 2006), these methods also enabled us to reveal the likely contribution of functional interpolation to perceptual continuity across scotomas generated by retinal lesions (Fiorani et al. 1992, 2003). RF quantification was performed using a fully automated, quantitative method to avoid bias, particularly due to the difficulties in delimiting the RFs of many cells within the LPZs (Waleszczyk et al. 2003). The parameters we quantified were the orderliness of topography (scatter), the RF area, and the strength of the response for each eye. We then compared the results obtained after stimulation of the lesioned eye with those following stimulation of the control (nonlesioned) eye.

Materials and Methods

We conducted experiments on 4 adult *Cebus apella* monkeys weighing 2–3 kg. The *Cebus* is a diurnal, medium-sized New World primate,

comparable to the Old World monkey *Macaca fascicularis* in terms of brain size, sulcal pattern (Le Gros Clark 1959; Freese and Oppenheimer 1981), and retinotopic organization of V1 (Gattass et al. 1987). All experimental protocols were conducted in accordance with the NIH guidelines (NIH publication no. 86-23, revised 1987) for animal research and were approved by the Committee for Animal Care and Use of the Instituto de Biofísica Carlos Chagas Filho, Universidade Federal do Rio de Janeiro.

Initially, the animals were anesthetized with an intramuscular administration of a 1:5 mixture of 6% ketamine hydrochloride (Ketalar; ParkeDavis) and 2% dihydrotiazine hydrochloride (Rompum; Bayer). Atropine sulfate (0.15 mg/kg) and benzodiazepine (0.8 mg/kg) were also administered to reduce secretions. The pupils were dilated with 2 drops of 1% tropicamide and the retina inspected using an ophthalmoscope (American Optical Company, Buffalo, NY, United States of America). Only animals without retinal pathologies were used.

Electrophysiological Recordings

The maintenance and monitoring of the animals during the recording sessions followed procedures detailed previously by Rosa et al. (1993). Briefly, prior to the recording session, a bolt for head fixation in a stereotaxic apparatus and a recording chamber were implanted in the skull, under anesthesia and aseptic conditions. Brain edema was prevented by the administration of dexamethasone phosphate (0.3 mg/kg, intra muscular) 2 h prior to the recording session followed by additional doses every 6 h. Anesthesia was maintained with a mixture of 70% nitrous oxide and 30% oxygen, combined with a continuous intravenous infusion of fentanyl citrate (0.03 mg/kg/h). Animals were also immobilized with pancuronium bromide (0.1 mg/kg/h) and kept under artificial mechanical ventilation. Body temperature, electrocardiogram, and end-tidal CO_2 were monitored continuously. Cycloplegia was produced using 10% phenylephrine, and pupils were dilated with 1% tropicamide. Contact lenses of appropriate curvature were used to focus the eyes on the screen of a computer display and also to protect the corneas.

Arrays of tungsten microelectrodes (1 MΩ impedance at 1 kHz) were used to record the extracellular neuronal activities. In 3 animals (M1–M3), we used 16 microelectrodes arranged in a regular 4-by-4 array, with a separation of 1.4 mm between electrodes. In animal M4, we used 32 microelectrodes arranged in a 4-6-6-6-6-4 array, with a separation of 0.7 mm between electrodes. After craniotomy, the dura mater was removed and the microelectrode array was carefully angled so that each electrode would penetrate approximately perpendicular to the cortical surface. The exposed cortex was then protected with a layer of silicone oil. In this experiment, we aimed to record from an array of electrodes with tips located close to layers 5-4 in the calcarine cortex. The array was angled and positioned as the electrodes would penetrate the calcarine cortex, orthogonal to its surface, along a cortical column. The microelectrode array was then advanced in 200 µm steps. The neuronal activity was recorded at each step to monitor the topographic transition from the opercular surface to the roof of the calcarine sulcus, which was the region of interest in this study. We stopped the vertical progression of the electrode array when the monitoring electrode recorded the first transition from central RF (typically around 5°) to peripheral (14–18°) RFs. At this point, the movement of the electrode array was stopped and the electrodes were kept at that location for at least 30 min, to allow stabilization. After reaching the roof of the calcarine sulcus, the array was advanced slowly in 50 µm steps into the gray matter and we monitor the RFs corresponding to each electrode. We continued advancing the electrodes until virtually all electrodes recorded consistent peripheral RFs. Typically, this location was 200–400 µm deep into the calcarine cortex, around layers 5-4. From this point on, we do not move the electrodes and we recorded the neuronal activity continuously in blocks of 10–15 trials for each eye and for each method. Small vertical movements of the electrodes resulted on 2 RFs before the lesion and up to 5 RFs after the lesion. We continued to record after the lesion for at least 6 h to account, in part, for the cells located along the same columns (Rosa et al. 1992). These repeated measurements were later used for estimates of RF scatter in the columns. Although the array remained at the same stereotaxic position, we cannot rule out small progressions of the electrodes into the cortex, along a cortical column.

For each electrode, we recorded the RF positions for an average of 2 recording sites (defined by different electrode depths) before the lesion, and 6 recording sites after the lesion. At each of these sites, we recorded the activity of small groups of neurons (typically 2 or 3) separately for each eye, before and after the retinal lesion. Further, the responses were characterized using 2 stimulus paradigms (small discreet stimulus and long moving bars—described below) for 2 blocks of the 10–15 trial before the lesion and 5 blocks after the lesion. Thus, on average, for each electrode in the arrays, we mapped 7 RFs with each stimulus paradigm, for each eye (14 RFs). After eliminating from the sample recording sites that yielded poor or no responses, we were able to conduct analyses based on 1774 RFs, recorded at 444 recording sites in 4 animals.

The multiunit signals were amplified and filtered between 0.7 and 5.9 kHz (HST/16o25 headset, 32-channel pre-amplifier box, Plexon, Dallas, TX, United States of America) before being digitized at 32 kHz by a high-speed, 16-bit resolution A/D card (PCI-6259, National Instruments, Austin, TX, United States of America). Experimental control, stimulus generation, and synchronization were based on the CORTEX program (NIH, Bethesda, MD, United States of America); while the signal online display, as well as data acquisition and storage, was controlled by custom written software (SPASS, Max-Planck Institute, Frankfurt, Germany).

Neuronal Activity Normalization—Signal-to-Noise Ratio

To compare RFs with different neuronal firing rates, we normalized the neuronal responses using a signal-to-noise ratio algorithm (S/N). The S/N represents the difference between the mean neuronal response, measured in standard deviation, and the response rate. This ratio was obtained by subtracting the mean neuronal activity from the original response and dividing the result by the standard deviation of the original response. This procedure is essentially similar to calculating the z-score of a sample ($zx = x - \mu x/\delta x$). This procedure allowed us to compare the size and location of multiunit RFs mapped with the automatic methods describe below. Changes in the spike sorting threshold, allowing selecting different multiunit recordings, at the same locations, revealed no change in RF size or location. Multiunits with different firing rates recorded at the same location showed also similar RFs.

Mapping of RFs

RF maps were obtained, both prior to and following retinal lesioning, by presenting stimuli on a screen monitor (LCD, Philips) placed 57.3 cm in front of the animals' eyes. We used 2 mapping procedures for local and global mappings. We based the local method on reverse correlation of the location of a small white square (0.5° × 0.5°) that flickered at 60 Hz in a 15° × 15° panel. This panel was subdivided into 900 small squares (0.5° × 0.5°), and at the end of each trial (15 s) all 900 positions had been stimulated (Botelho et al. 2007). The responses of the cells were computed for 30 presentations of the stimulus, in each position, producing a 2-dimensional (2D) array map (spatial map) that was smoothed by a 2D convolution of a 2.5-degree Gaussian window.

For global mapping, we used white, 30° × 0.3° bars moving across the screen at the speed of 10°/s (total excursion, 30°) in 8 (0°, 45°, 90°,…315°) or 12 (0°, 30°, 60°,…330°) directions. Figure 1 shows the steps used to automatically map the RFs with long moving bars. The RF automatic mapping procedure was based on computing the latency-corrected neuronal activity in response to elongated bars moving in 1 of the 8 or 12 directions of motion. Initially, peristimulus time histograms (PSTHs) were computed based on 10 stimulus presentations, using a bin width of 10 ms. Figure 1*A* illustrates the PSTHs of a single unit in response to bars moving at 90° and 270°. Single-trial spike trains used to produce the PSTHs were aligned to the stimulus onset. The PSTHs were then smoothed, using a normal convolution filter of 120 ms time-window, resulting in the time-spike density function (TSDF). The TSDF characterizes the dynamics of

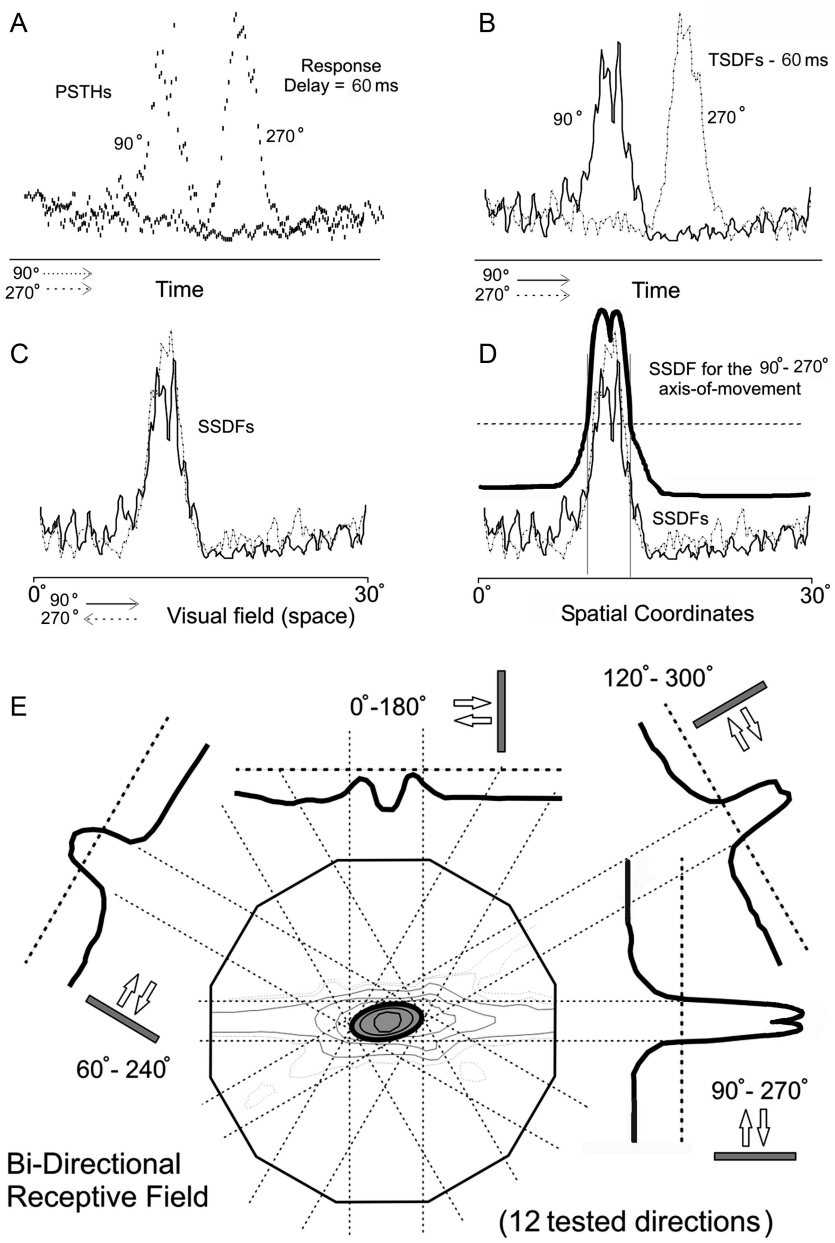

Figure 1. Steps used to determine PSTHs, SDFs and to locate the center and the borders of the RFs in a quantitative intersection map. (*A*) PSTHs; (*B*) time SDFs—60 ms delay; (C) space SDFs (in spatial coordinates: Mirrored along the vertical axis); (*D*) mean SSDF for each axis of movement; (*E*) quantitative intersection map based on 12 tested directions (for details, see text).

neuronal firing pattern, as it is a continuous and derivable function (Fig. 1*B*). To enable the transformation of the TSDF into the space-spike density function (SSDF), we were required to estimate the response latency of the neuron, and thereby correct the TSDF accordingly. As can be seen in Figure 1*B*,*C*, the TSDFs (thin and dotted lines for the 0° and 180° directions of motion, respectively) were shifted forward in time, corresponding to the estimated 60 ms response latency of the neuron. For the SSDF, this corresponds to a correction in the space domain. Thus, to integrate the spike density functions (SDFs) at the space domain, the time-corrected functions obtained for bars moving in opposite directions were flipped along the horizontal axis (Fig. 1*D*), resulting in a homogeneous space function. Thus, we computed SDFs for each direction by averaging the histograms (bin width, 10 ms) for 10 presentations in each direction and after convolving with a 120-ms (or 1.2°) Gaussian window filter. After a 60-ms correction for latencies and for the spread of the neuronal responses throughout the stimulus length in the proper orientation, the SDF for each direction of movement was converted into a 2D distribution of the spike density in spatial coordinates (orientation response map). The average of the orientation response maps for all 8 tested directions resulted in a quantitative intersection map that shows the size and the location of the RF (Fiorani et al. 2001; Azzi 2004; Soares et al. 2004; Botelho et al. 2007). Eight or 12 orientation response maps were combined to build a 3D representation of the neuronal response in the global paradigm (Fig. 2*A*). We obtained a 2D, color-coded representation of the RF by flattening the 3D representation (Fig. 2*B*).

To serve as reference points, at the start of each recording session, we projected the borders of the optic disc and the center of the fovea of both eyes onto the stimulation screen using a reversible ophthalmoscope. We checked these reference points several times during the experiment to rule out eye movements. To correct the misalignment (translation and rotation) of the optic axes of the eyes caused by the neuromuscular blockage, we used a rigid transformation (a minimum square method) to adjust the coordinates of all RFs from one eye to

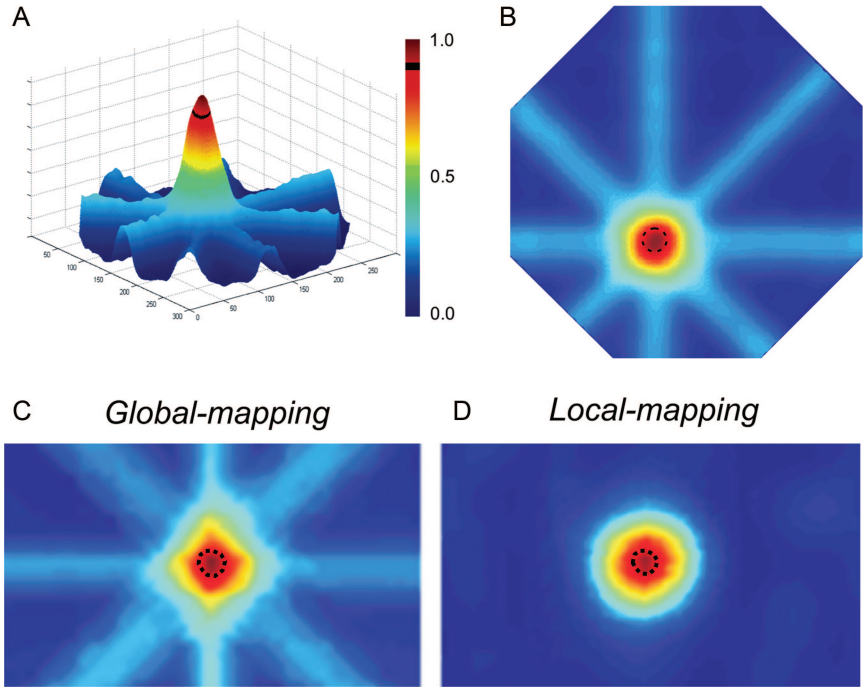

Figure 2. Multidimensional representation of bias-free RF mapping. (*A*) Three-dimensional representation of the neuronal response (quantitative intersection map) elicited by a thin bar moving in 8 directions (global mapping). (*B*) Color-coded, 2D representation of the quantitative intersection map used to determine the size and location of the RFs (dashed circle), using a peak criterion of 90%. (*C* and *D*) Comparison of RF size and location using the global (*C*) and local (*D*) visual stimulation methods (for details, see text).

the corresponding RFs from the other eye. For this binocular matching procedure, we used the normal eye RFs as reference and adjusted the RF coordinates of the lesioned eye. In one case (animal M4, Fig. 8), the eyes were quite misaligned leading to less precise superimposition of the RFs of both eyes due to tangent distortions (see animal M4, Fig. 8).

We defined RF borders as polygons by applying a threshold of 90% of the map peak response value for both local and global mappings (Fig. 2). We chose this threshold value, together with the width of the Gaussian filters to match the size of the neuronal responses. First, we defined a Gaussian filter width (1.2°) for the global mapping to give a RF size (90% peak activity) similar to the width of the SDF at half-peak. Due to the local mapping low resolution, a 0.5° pixel, we empirically defined a Gaussian filter width (2.5°) to give a RF size (90% peak activity) similar to the one obtained by the global mapping. Examples of RFs of one V1 neuron mapped with local and global visual stimulations are illustrated in Figure 2*C*,*D*, respectively.

The RF scatter was defined as the distance of each individual RF center relative to its expected position, which we determined as the average RF center position for all the RFs obtained in the same electrode before lesioning, for both eyes, and for the control eye, after lesioning.

The steps used to generate maps of locations and sizes of RFs in V1, for each eye, are illustrated in Figure 3. Selected recording sites (10–12 and 14–16) from the animal illustrated in Figure 5 are shown in Figure 3. Automated RFs mapped with long moving bars (global) are illustrated in a projection of the right and left retina (Fig. 3*A*). The borders and location of the RFs corresponding to each eye are illustrated in Figure 3*B*,*C* (right and left eyes, respectively).

Retinal Lesions

We planned the retinal lesions around the temporal horizontal meridian (HM) to minimize damaging of ganglion cell axons (Airaksinen and Tuulonen 1993). We applied several pulses of infrared laser, 1 W for 1 s to create lesions on the right eye. The laser lesions caused local cell destruction of all retinal layers (Fig. 3), preserving the passing ganglion cell axons. Table 1 summarizes the spatial location of the lesion, measured as the distance between the center of the fovea and the medial lesion border along the HM, and the lesion size, height versus width, for each animal. In animal M4, as a result of unintentional vascular damage, the lesion size was 16.6° × 6.6°, with a medial border located at 3° eccentricity along the HM. We planned these lesions so that the microelectrode array in V1 would be partially inside and partially outside the LPZ. The efficacy of the lesion was immediately ascertained by mapping the scotoma using the local mapping method. The preservation of the ganglion cell axons was inferred in case M1 that had the retinal lesion located nasal to the representation of the recording array. In this case, the responses outside the lesion were similar for both eyes.

Conversion From Visual to Cortical Coordinates (Monopole Mapping)

To quantify the extent of cortical reorganization in V1 after retinal lesioning, we used a monopole mapping technique (Polimeni et al. 2006), which converts the visual field maps (in degrees) to cortical V1 maps (in millimeters). To carry out this procedure, we used a complex logarithmic function: $w = k \log (z + a)$; $z = x + iy$, where x and y correspond to a point in the visual field; the parameter a defines the size of the foveal representation in V1; and the parameter k adjusts the V1 area. To match the cortical monopole map to the experimentally derived map of V1 in the *Cebus* monkey (Gattass et al. 1987), we used the empirically determined values of 0.01 and 10 for parameters a and k, respectively. Besides giving the measurements in cortical distance (mm), the monopole transformation also compensates partially for the variations associated with eccentricity observed in the topography (cortical magnification factor), scatter, and RF size in V1 (McIlwain 1976; Gattass et al. 1987). Consequently, most of the figures in this paper represent the visual RFs in cortical coordinates (cortical representation of receptive fields, CRRF). We use the term eccentricity (Ecc) to refer to the distance from the fovea both in the visual field (in degrees) and in the cortex (in mm). We converted the coordinates of the left visual field, where we mapped the RFs, to the right visual field by taking the absolute value of the x coordinate (horizontal flip) because the monopole logarithmic transformation is

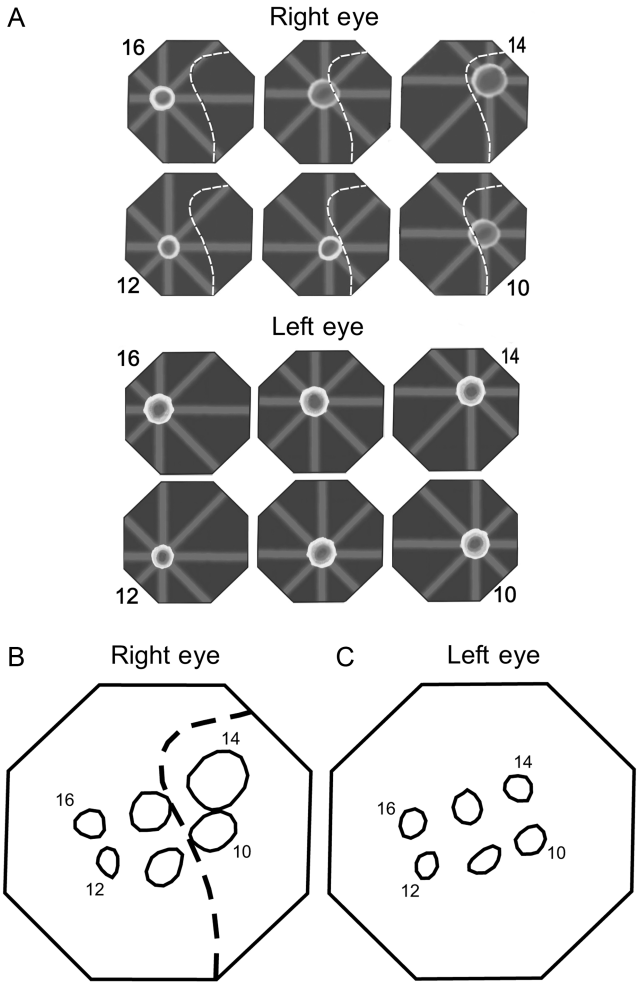

Figure 3. Steps used to generate bias-free maps of locations and sizes of RFs in V1, for each eye. RFs mapped with long moving bars (global method) are illustrated using a projection of the right and left retina (*A*). The location and the borders of the RFs corresponding to the right eye are illustrated in (*B*), while those corresponding to the left eye are shown in (*C*).

Table 1
Spatial location of the lesion measured as the distance between the center of the fovea and the lesion size for each animal

Animal	Lesion eccentricity (°)	Lesion size—height × width
M1	5.0	9.5° × 5.7°
M2	7.6	6.0° × 7.5°
M3	5.0	8.0° × 7.0°
M4	3.3	6.6° × 16.6°

incompatible with negative numbers. Thus, we have used horizontally flipped representations of the visual field throughout this paper.

To project the retinal lesion borders to the cortical monopole map, we used a post-mortem image of the fundus of the eye to mark the centers of the fovea and optic disc and to draw the contour of the lesion (Fig. 4*A*). As for the visual coordinates, we configured the retinal image in Figure 4*A* flipped horizontally because the incompatibility of the logarithmic transformation with negative numbers. We used the fovea and the center of the optic disc as references (0 and 15° Ecc, respectively) to define the horizontal and vertical meridians and the retinal coordinates. The retinal lesion representation onto the visual field is seen in Figure 4*B*, and it's representation onto the cortical map using the monopole transformation is shown in Figure 4*D*.

Histological Analysis

At the end of the recording session, the animals were deeply anaesthetized with sodium pentobarbitone (30 mg/kg) and perfused intracardially with normal saline followed by 2% of paraformaldehyde in phosphate buffered saline (PBS); 2% of paraformaldehyde in PBS + 2.5% glycerol; PBS + 5% glycerol; and PBS + 10% glycerol. Serial 40 μm parassagital sections were obtained using a cryostat. The electrode tracks were reconstructed in a drawing of histological sections stained alternately for cell bodies (with cresyl violet) and for cytocrome oxidase (CytOx; Silverman and Tootell 1987).

After perfusion, the anterior chamber of the lesioned eye was removed, and a digital photograph of the eye fundus was obtained. The retinas were cut parallel to the HM, at 30 μm thickness, and stained with neutral red.

Results

The results are based on the quantitative mapping of 1774 V1 RFs from 444 recording sites in 4 adult *Cebus* monkeys. First, we will qualitatively compare the topographic maps obtained with the fully automated, bias-free quantitative mapping methods both before and after the retinal lesioning, followed by a quantitative analysis of RF size, scatter, and S/N ratio.

Topographic Maps Before Retinal Lesioning

Prior to the lesion of the retina, with the electrode array in the position, we determined the size and location of RFs of the neuronal clusters in V1 under control conditions by using both local and global mapping methods. Typically, we mapped 2 times with each method before the lesion. The results from 1 experiment are shown in Figure 5. Figure 5*A* illustrates the averaged RFs of the right eye recorded with the electrode array in animal M1 mapped with the local (continuous line) and global (dotted line) methods. We illustrate the average RFs, because the scatter and size variation are small. The RFs mapped with both methods were overlaid, with the exception of electrode 4, where the RF could not be determined with the local mapping method. Figure 5*B* shows the CRRFs of the averaged RFs illustrated in *A* after the monopole transformation. Following this transformation, the lower and upper visual fields are represented dorsally and ventrally, respectively. In addition, the distortion of the electrode array as a result of the cortical magnification factor and the increase in RF size as a consequence of eccentricity are now strongly reduced in the CRRFs as shown in Figure 5*B*. Comparison between the mean RFs (and CRRFs) for the control eye (dashed) and for the eye that was subsequently lesioned (continuous) mapped with both local (Fig. 6*A*,*B*) and global (Fig. 6*C*,*D*) methods shows no significant changes in size or location of the mean RFs (and CRRFs) after the application of the binocular alignment procedure. Only one of the mean RFs (and CRRFs, site 8) was not properly matched, probably due to its proximity to the control eye's optic disc.

Topographic Maps After Retinal Lesioning

After retinal lesioning in the right eye, the RFs mapped for the control (left) eye maintained their original positions, with similar results obtained for both mapping methods. By contrast, the RFs representing the visual field of the lesioned eye displayed reorganization, the nature of which depended on the mapping method. Figure 7 compares the CRRFs of both eyes of animals M1 (*A* and *B*) and M2 (*C* and *D*) for both mapping methods in the cortical monopole projection. The

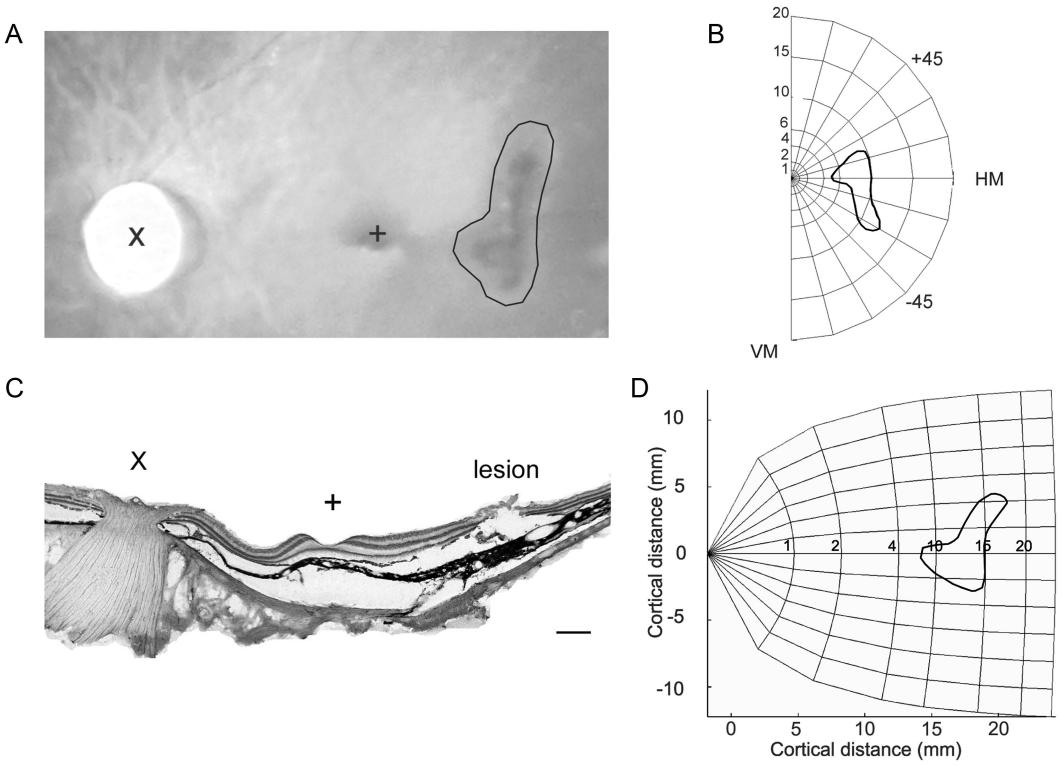

Figure 4. Retinal lesion in animal M1. (*A*) Delineation of the retinal lesion in a horizontally flipped image (see Materials and Methods) of the fundus of the lesioned (right) eye. For reference, the center of the optic disc (x) and the center of the fovea (+) are labeled. (*B*) Representation of the lesion illustrated in *A* in the visual hemi-field. (*C*) Image of a horizontal section of a lesioned retina stained with neutral red. Scale bar = 500 μm. (*D*) Schematic monopole mapping of V1 showing the visual topography and the limits of the retinal lesion. VM, vertical meridian; HM, horizontal meridian.

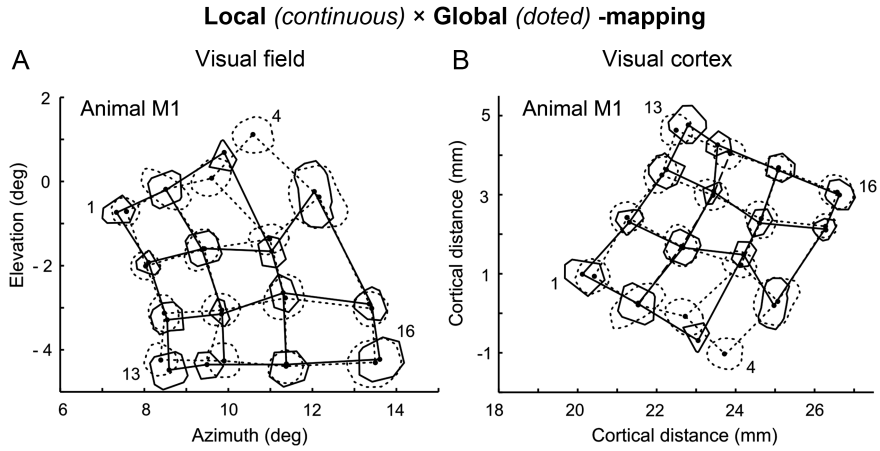

Figure 5. Comparison of the 2 mapping methods on the visual field and on the cortical monopole representation. (*A*) Visual field representation of average RFs mapped with the right eye before lesioning of animal M1 using the local (continuous line) and global (dotted line) mapping methods. (*B*) CRRFs generated by the monopole transformation of the coordinates illustrated in *A*.

control and lesioned eyes were stimulated 6 h after retinal lesioning, and we mapped CRRF with both mapping methods. After the lesion, some mean CRRFs were displaced from its original position, inside of the LPZ, toward regions of the undamaged retina (arrows), while others remained inside the LPZ (open circles). The 2 mapping methods showed different results. While the local mapping only revealed CRRF at locations corresponding to the undamaged regions, the global -mapping showed many interpolated CRRF inside the LPZ.

Figure 8 illustrates contours of individual RFs of animal M4 before and after the lesion, in visuotopic coordinates. Note that here every RF contour was drawn, while in the following figure we only show the location of the center of the averaged CRRFs (typically, average of 3 CRRFs). As mentioned previously, while the visual field representation is anisotropic, (Gattass et al. 1987), the cortical representation is suitable to direct measurements, in mm, of RF displacements and scatter. Thus, the changes observed with this representation can be directly related to changes in connectivity.

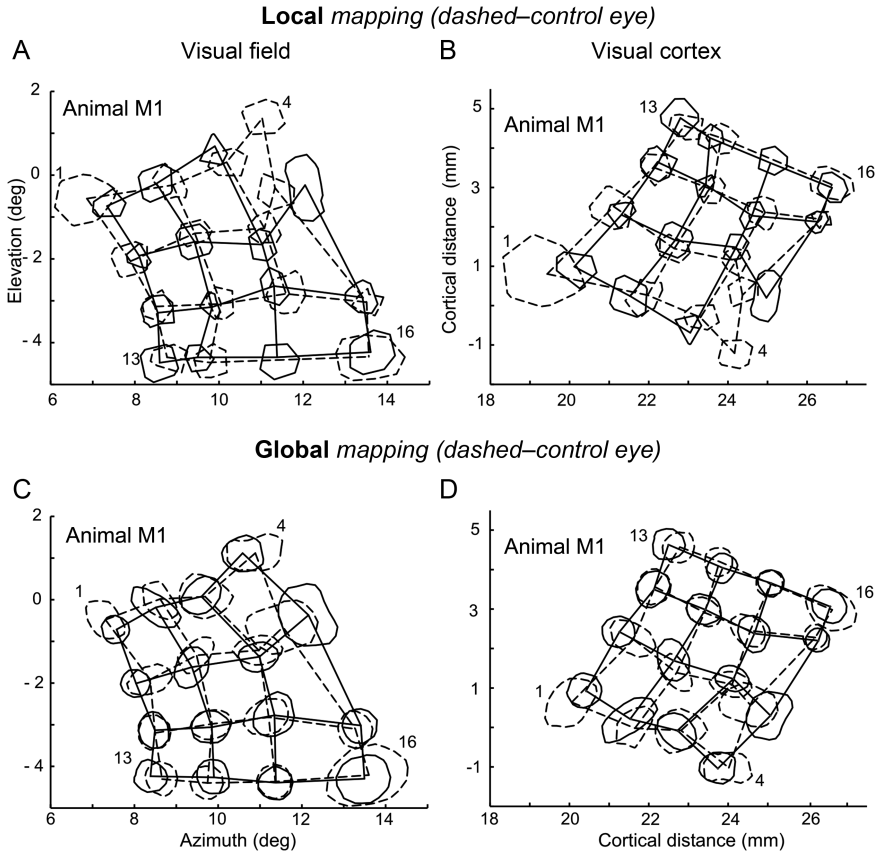

Figure 6. Topographic organization of RFs recorded at the dorsal calcarine bank before the retinal lesion. Visual field (*A* and *C*) and cortical (*B* and *D*) representations of RFs from animal M1 mapped through the right eye (continuous line) and the left control eye (dashed) with local (*A* and *B*) and global (*C* and *D*) mapping methods.

Figure 8 illustrates 521 RFs plotted automatically. The fields corresponding to sites located inside the LPZ were drawn in red, while those located outside the projection of the lesion were drawn in blue. Figure 8 shows very different results for global and local mapping methods. When using the local mapping method, recording sites corresponding to the representation of the blind spot (of the control eye) or to the representation of the lesion (of the lesioned eye) either does not reveal RFs at those locations or reveal displaced RFs. In contrast, with the global method RFs were found inside the representations of both the blind spot and lesion.

We mapped 290 RFs before the lesion and 231 RFs after the lesion. Based on the location of RF centers, we found, after the lesion, 71 RFs inside the lesion with the global mapping, and 33 with the local mapping procedure. Note that with the array at the same retinotopic position, we had mapped 127 RFs before the lesion with the global mapping and 68 with the local mapping procedure at the same location.

Figure 9 illustrates individual CRRF centers using the local (*A* and *C*) and global (*B* and *D*) mapping methods for animals M1 and M4. The CRRFs driven by the control eye (black open circles) showed the expected topography and a small scatter. In the case of animal M4, recording sites 1, 2, 5, 6, and 7 were inside the cortical representation of the optic disc and, as expected, did not yield RFs when the local mapping method was used. The optic disc representation of the control eye was superimposed onto part of the LPZ, producing a binocular scotoma. Inside the LPZ, most cells stopped responding to local stimuli through the lesioned eye (filled circles), and, as expected, no CRRF was mapped. Only cells near the LPZ border of the lesioned eye continued to respond to stimulation. Their CRRFs (red filled circles) were displaced in such a way that they covered the undamaged retina (animal M1: Sites 3 and 10; animal M4 Sites 3, 8, 14, 19, 23, 25, and 26). In addition, some of the CRRFs originally located just outside the lesion were slightly displaced (animal M4: RFs 9, 15, 21, 27, and 31). In contrast, CRRFs that covered portions of the retina outside the lesion borders remained in their original position (black filled circles), overlapping with the CRRFs mapped through the control eye.

With the global mapping procedure (Fig. 9*B*,*D*), the CRRFs mapped by stimulating the control eye (black open circles) kept their approximate original positions after lesioning, which was similar to the results observed using local mapping. The main difference observed between local and global mappings through the control eye is seen in the case of animal M4 (Fig. 9*C*,*D*), which shows many mapped (intersected) responses inside the optic disc representation with a very good overall topography (small scatter—black open and filled circles); these can only be mapped with the global stimuli. In addition, unlike the local mapping method, the global mapping revealed responses to the lesioned eye (filled circles) in recording sites located further inside the LPZ (Fig. 9*B*,*D*, red filled circles). Moreover, there was a greater variation in the pattern of CRRF displacement revealed by this method: 1) Some CRRFs originally located within the lesion remained in a similar position, showing, however, a larger scatter than the CRRFs obtained through the control eye

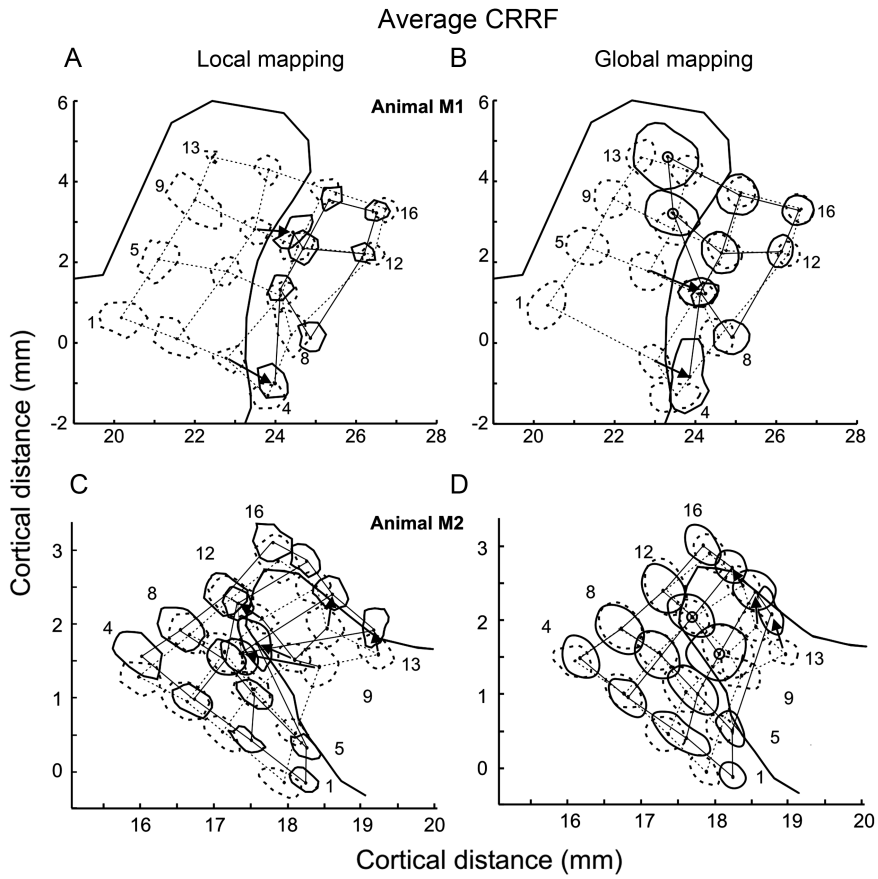

Figure 7. Cortical reorganization after retinal lesion: Average CRRFs. CRRFs mapped through the control (dashed) and lesioned eyes (continuous) in animals M1 (*A* and *B*) and M2 (*C* and *D*) with local (*A* and *C*) and global (*B* and *D*) mapping methods. Arrows points to the RFs that moved to the border of the lesion, avoiding the LPZ. Open circles mark the center of RFs that remained inside the LPZ.

(animal M1: Sites 10 and 14; animal M4: Sites 1, 2, 11, 12, 13, 14, 25, and 30); 2) some CRRFs located near the internal border of the LPZ showed a tendency to be displaced to just outside the LPZ in a way that was similar to that observed with local mapping (animal M1: Sites 3 and 6; animal M4: sites 3, 8, 20, and 26); and 3) some CRRFs located close to the external border of the LPZ tended to be displaced to the inside of the LPZ (animal M4: Sites 9 and 15) or to a more distant region of the LPZ external border (animal M4: Site 31). The CRRFs located farther from the external border of the LPZ tended to remain in the same positions. In animal M1, site 2 was not responsive to the control eye stimulation, while sites 1, 2, 4, 5, and 9 were not responsive to the lesioned eye stimulation. In animal M4, site 6 did not respond to stimulation of either the control or the lesioned eye, while sites 7, 24, and 29 were responsive to stimulation of the control eye only. Thus, this figure shows the difference in scatter between sites inside and outside the LPZ by comparing the red and black filled circles. This figure also illustrates the difference between the 2 mapping methods for sites inside the LPZ, by comparing the red filled circles from the local and global mapping methods. These differences are also seen for the other animals studied.

Cortical Representation of RF and RF Areas

We compared the area and scatter of the RF and CRRFs mapped for the lesioned and the control eyes before and after retinal lesioning (Table 2 and Fig. 10). RFs and CRRFs located both inside and outside of the LPZ were quantified using both mapping methods. Measurements were made with the local mapping method, outside the lesion, for the control (n = 120) and lesioned eyes (n = 125), as well as inside the lesion for the control (n = 150) and lesioned eyes (n = 59). They were also made with global mapping outside the lesion for control (n = 158) and lesioned eyes (n = 151) as well as inside the lesion for control (n = 238) and lesioned eyes (n = 135). A total of 1136 RFs were used for this and subsequent analyses. In animals M1, M3, and M4, the electrodes outside of the LPZ were located more peripherally (temporal) to the lesion, while, in animal M2, they were located between the lesion and the fovea.

The RF size is known to increase with eccentricity, and even after the monopole transformation, the CRRF size is not constant along the eccentricities. We found a positive correlation between the RF area and the visual eccentricity (RF area = 0.034 Ecc + 0.135; r = 0.42; n = 1774), and a negative correlation between the CRRF area and the cortical eccentricity (CRRF area = –0.047 Ecc + 1.59, r = –0.47, n = 1774). To calculate the regressions, data from all areas, both eyes, pre- and post-lesion, in and outside the lesion were pooled. To avoid the variance introduced by the eccentricity range in this study (around 18–31 mm in the cortex or 6–22° in the visual field), we used the predicted areas compensated for eccentricity to compare CRRFs and RFs sizes. We obtained the CRRF and RF eccentricity-compensated "areal variations" by

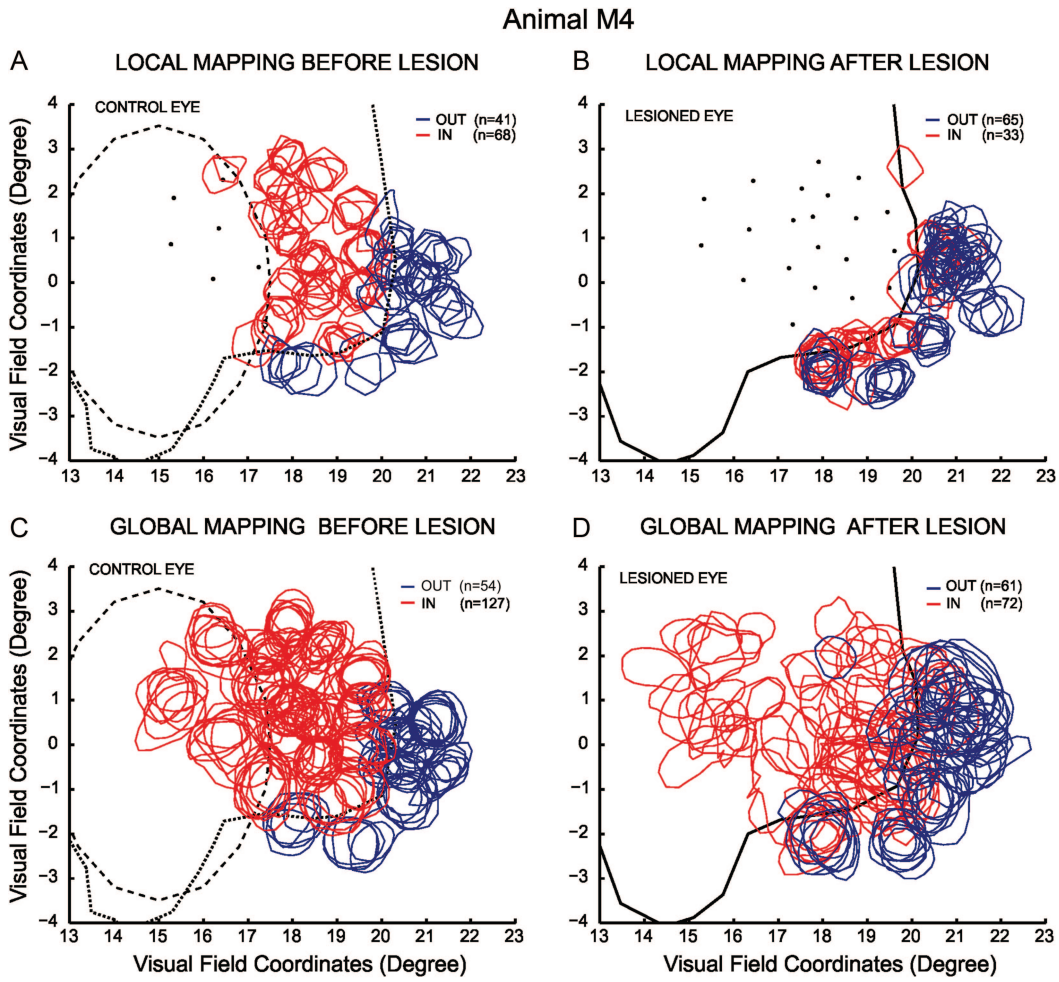

Figure 8. Cortical reorganization after retinal lesion: RF borders mapped through the control (left: *A* and *C*) and lesioned eyes (right: *B* and *D*) in animal M4 with local (*A* and *B*) and global (*C* and *D*) mapping methods. RF borders from sites inside the LPZ are show in red, while those from sites outside the LPZ, in blue. The images show the individual RFs and their expected positions in the visual field. The thick line represents the anatomical borders of the LPZ, the dotted line is a projection of the border of the LPZ, and the dashed line the optic disc border.

measuring the difference between the CRRF and RF areas and the regression line fitted as a function of eccentricity.

As expected, before retinal lesioning, there were no significant differences between lesioned and control eyes in the area variance of the CRRFs and RFs mapped with the local and global mapping methods, inside and outside of the expected LPZ (Table 2). However, after retinal lesioning, we found different results for the area variance between lesioned and control, depending on the mapping method used. With local mapping, the CRRF areas remained unchanged in both regions, both outside (Fig. 10*A*) and inside the LPZ (Fig. 10*B*). On the other hand, with global mapping, the CRRFs and the RFs mapped through the lesioned eye were larger than the RFs mapped through the control eye, both inside and outside the LPZ (Fig. 10*C*,*D* and Table 2).

Scatter

Scatter is also known to be correlated with eccentricity (Hubel and Wiesel 1974). However, in this study, we did not make an eccentricity correction because the correlation in our data was very low and not significant (cortical scatter [in mm] = –0.012 Ecc + 0.533, $r = 0.178$ and visual field scatter [in degrees] = 0.001 Ecc + 0.146, $r = 0.155$, $n = 174$).

The scatter, before retinal lesioning, is similar between the eyes in both regions, inside and outside the expected LPZ with both mapping methods (Table 1), and the 2 mapping methods gave similar distributions (not shown), in the visual field and in the cortex.

Immediately after retinal lesioning and for at least up to 6 h, both mapping methods revealed that inside the LPZ, the scatter of the RFs and CRRFs (Table 2), mapped through the lesioned eye, was significantly larger (0.59 and 0.53 mm) than the one obtained through the control eye (0.12 and 0.11 mm, Fig. 11*B*,*D*). Furthermore, despite the significant qualitative differences in the maps of lesioned regions obtained with each mapping method (see Fig. 7), for the lesioned eye, the scatter medians and the distributions found with each method are very similar "inside" the LPZ (Fig. 11*B*,*D*). Outside the LPZ, only the global mapping method revealed a significant difference in the CRRFs' scatter between the lesioned and the control eyes (control = 0.11 mm, lesioned = 0.16 mm, Fig. 11*C*). Although statistically significant (see *P*-value), this difference is very small, the values are in the same range as

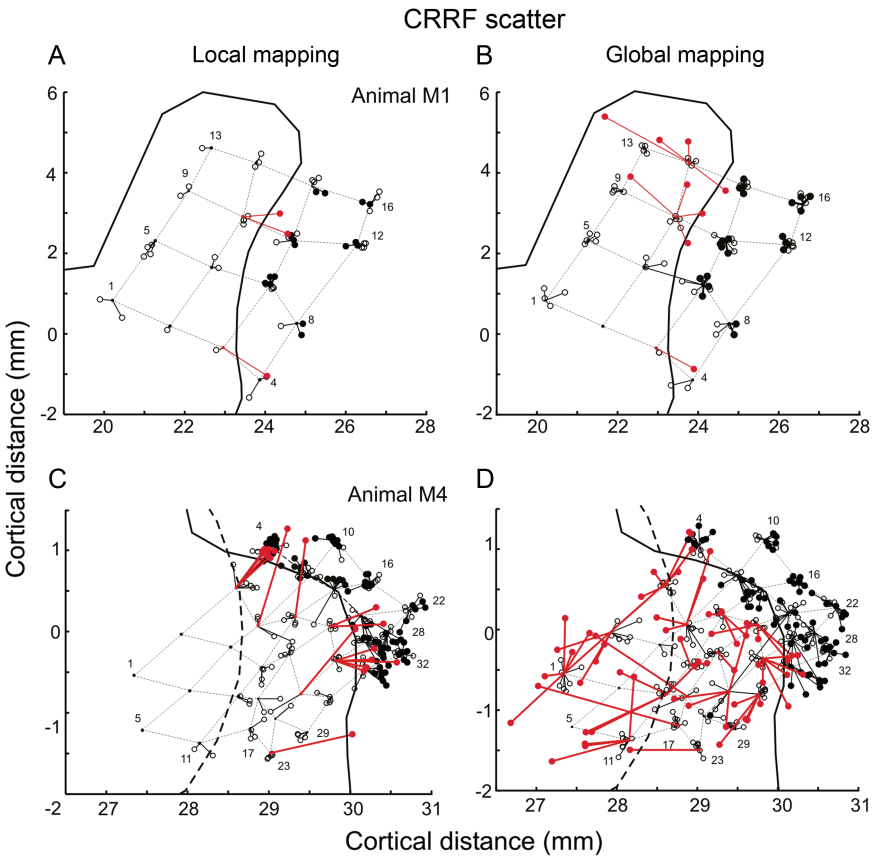

Figure 9. Cortical reorganization after retinal lesion: CRRF scatter. CRRFs centers mapped through the control (open circles) and lesioned eyes (filled circles) in animals M1 (*A* and *B*) and M4 (*C* and *D*) with local (*A* and *C*) and global (*B* and *D*) mapping methods. Individual RF centers from sites inside the LPZ are show in red, while those from sites outside the LPZ, in black. The images show the individual CRRFs centers connected to their expected positions (knots in the grid, with recording site numbers). The size of these connections represents the individual scatter of the CRRFs. The thick line represents the anatomical borders of the LPZ and the dashed line the optic disc border.

Table 2

Comparison of RF area and scatter and S/N ratio of the cells located outside (OUT) and inside (IN) the LPZ obtained with local and global mappings, through the lesioned (L) and control (C) eyes, both Pre- and Post-retinal lesions

	CRRF and RF area variance				CRRF and RF scatter				S/N ratio			
	Local		Global		Local		Global		Local		Global	
	C	L	C	L	C	L	C	L	C	L	C	L
Pre-lesioning												
OUT												
Cx	−0.10	−0.14	−0.04	−0.09	0.13	0.12	0.15	0.13	2.45	3.66	3.40	3.41
VF	−0.24	−0.21	−0.14	−0.11	0.18	0.18	0.16	0.14				
IN												
Cx	−0.09	−0.09	0.02	0.03	0.14	0.14	0.13	0.18	**2.59**	**3.50**	3.37	3.62
VF	−0.20	−0.17	0.03	0.06	0.18	0.21	0.19	0.18				
Post-lesioning												
OUT												
Cx	−0.08	−0.07	**−0.03**	**0.06**	0.14	0.14	**0.11**	**0.16**	2.97	2.91	3.46	3.23
VF	−0.17	−0.22	**−0.06**	**0.09**	0.17	0.17	**0.16**	**0.22**				
IN												
Cx	−0.08	−0.07	**0.05**	**0.09**	**0.12**	**0.59**	**0.11**	**0.53**	**2.98**	**2.56**	**3.40**	**2.48**
VF	−0.16	−0.22	**0.10**	**0.20**	**0.15**	**0.79**	**0.15**	**0.67**				

The significant differences ($P \leq 0.01$) are shown by the bold numbers. Areal variance, scatter, and S/N ratio were measured with the local mapping method, outside the lesion for control ($n = 120$) and lesioned eyes ($n = 125$) as well as inside the lesion for control ($n = 150$) and lesioned eyes ($n = 59$). These measurement were also made with global mapping outside the lesion for control ($n = 158$) and lesioned eyes ($n = 151$) as well as inside the lesion for control ($n = 238$) and lesioned eyes ($n = 135$). A total of 1136 RFs were used for this analysis.

Medians of CRRF and RF area variance and scatter analyzed in the cortex (Cx, in mm) and in the visual field (VF, in degrees), and the S/N ratio of the cells located outside (OUT) and inside (IN) the LPZ, comparing the stimulation of the control eye (C) with the stimulation of the lesioned eye (L), with the local and global mapping methods, Pre- and Post-retinal lesioning. The statistically significant differences ($P < 0.01$) are shown in bold.

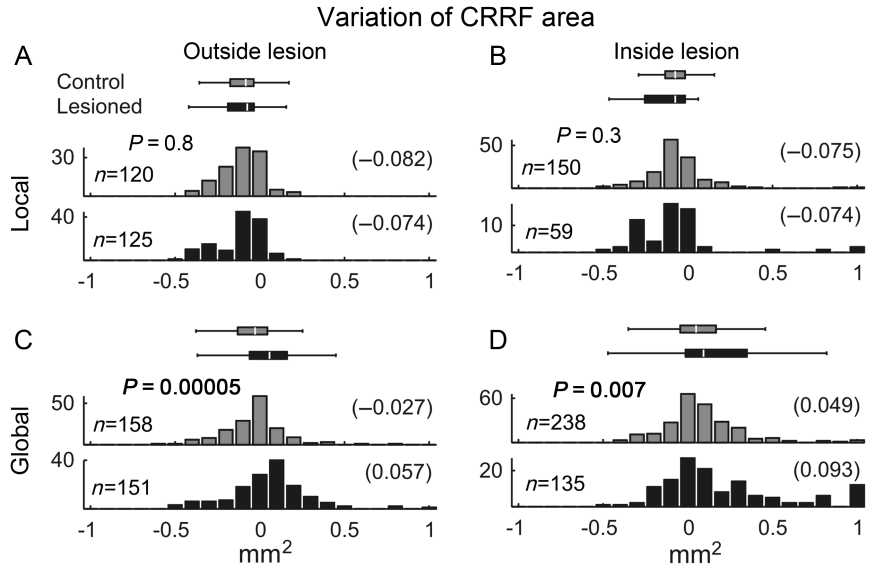

Figure 10. Quantitative analysis of CRRF area. The distribution (histograms) and the nonparametric statistics (box plots, on top) of the variation of CRRF area obtained with local and global mappings, through the lesioned eye (black) and through the control eye (gray), outside and inside the LPZ. (*A*) Areal variation of CRRFs measured with the local mapping method, outside the lesion, for control ($n = 120$) and lesioned eyes ($n = 125$). (*B*) With the local mapping inside the lesion for control ($n = 150$) and lesioned eyes ($n = 59$). (*C*) With global mapping outside the lesion for control ($n = 158$) and lesioned eyes ($n = 151$); and (*D*) with global mapping inside the lesion for control ($n = 238$) and lesioned eyes ($n = 135$). The medians (in parentheses) and the probability value (*P*) for nonparametric statistical difference are presented above to the histograms. Statistically significant probabilities ($P < 0.01$) are shown in bold.

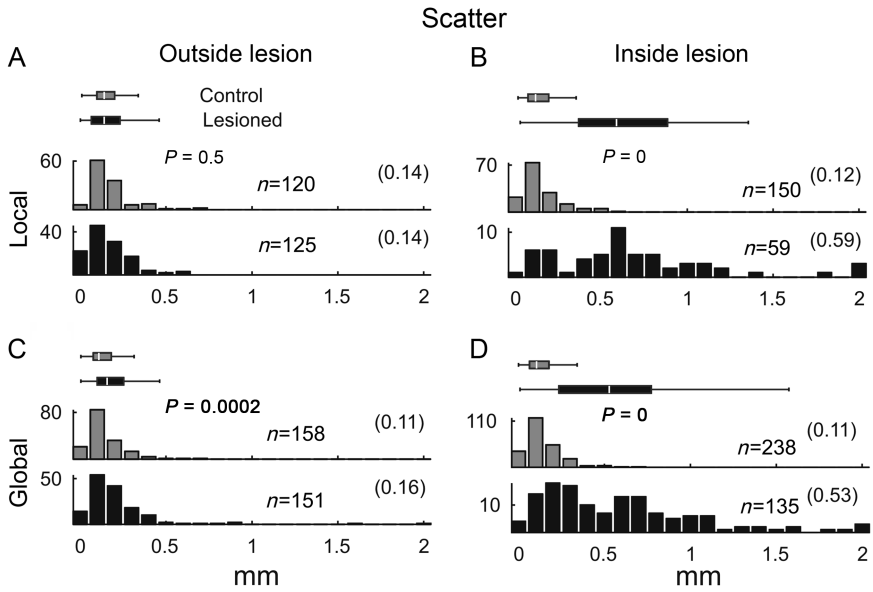

Figure 11. Quantitative analysis of CRRF scatter. The histograms and the nonparametric statistics (box plots, on top) of the scatter of the CRRFs obtained with local and global mappings, through the lesioned eye (black) and through the control eye (gray), outside and inside the LPZ. For conventions, see legend for Figure 10.

for the local mapping scatter outside the LPZ and in the pre-lesion scatter (0.14 mm, see above), and the distributions are very similar. This statistical significance appears to be incidental due to slight misalignments caused by the binocular matching procedure and the large sample of CRRFs obtained with global mapping (control $n = 158$, lesioned $n = 151$, Fig. 11*D*, see legend).

For the control eye, after lesioning, both methods showed similar scatter medians both inside and outside the LPZ (Table 2), and these values are in the same range as in the pre-lesion scatter and also as in the outside lesion scatter (post-lesioning).

Signal/Noise Ratio

The analysis of the S/N ratio provides further evidence of changes in neuronal excitability caused by retinal lesions. Prior to retinal lesioning, local mapping showed that cells inside the future LPZ had a significantly stronger response to the stimulation of the eye to be lesioned (ipsilateral) than they did to the stimulation of the control eye. A similar response pattern was observed using the global mapping method (Table 2), possibly due to the presence of the blind spot caused by the optic disc, a region dominated by the ipsilateral eye. We observed no significant differences outside the expected LPZ (Table 2).

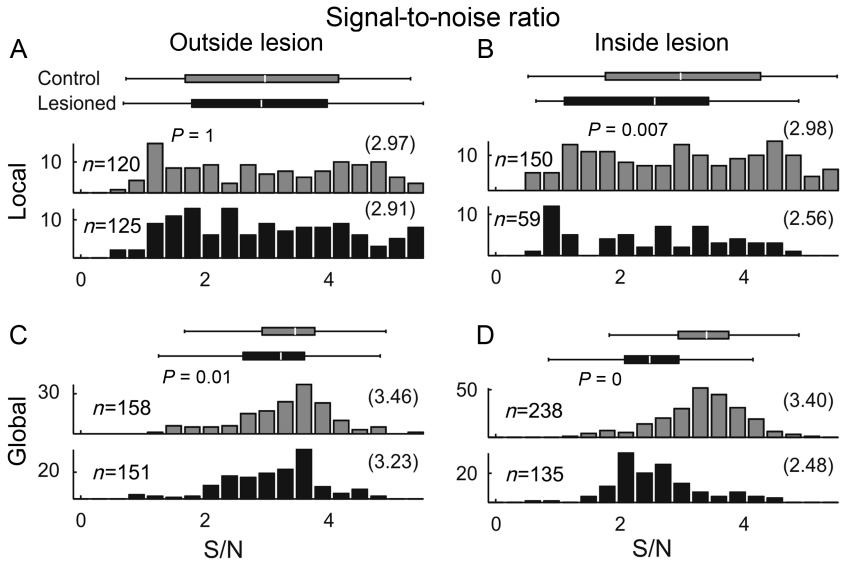

Figure 12. Quantitative analysis of signal/noise ratio. The histograms and the nonparametric statistics (box plots, on top) of the signal/noise ratio obtained with local and global mappings, through the lesioned eye (black) and through the control eye (gray), outside and inside the LPZ. For conventions, see legend for Figure 10.

After retinal lesioning, the remaining responsive clusters inside the LPZ showed significantly weaker responses to the stimulation of the lesioned eye than they did to the control eye for both mapping methods (Fig. 12*B*,*D*). Outside the LPZ, this difference is not observed for the local mapping (Fig. 12*A*), but slight weaker responses are seen for the lesioned eye with the global mapping (Fig. 12*C*).

Extent of the LPZ Reorganization

To quantify the extent of the reorganization within the LPZ, we measured the distances between the expected CRRF centers (see Materials and Methods) of the responsive recording sites inside the LPZ and the closest lesion border mapped through the lesioned eye. Across all animals, the largest cortical distances between the lesion border and the recording sites measured with the local mapping method were 0.85 and 0.78 mm (Fig. 9). With the global mapping method, on the other hand, we found responsive recording sites in the range of 1.87 and 1.79 mm (Fig. 9).

We also analyzed the number of recording sites responding to stimulation inside the region of the visual field corresponding to the retinal lesion immediately and up to 6 h following retinal lesioning. Before retinal lesioning, 39 sites responded to both local and global mapping "stimuli", but immediately after lesioning, only 16 sites (41%) and 34 microelectrodes (87.18%) responded to local and global mapping, respectively. These results remained unchanged throughout the recording session.

Discussion

The main conclusions from this study are that a topographic cortical reorganization can be seen shortly after monocular retinal lesions and that the measurable extent of the reorganization depends on the mapping method used, local or global. Additionally, the 5-fold increase in the scatter of the CRRFs inside the LPZ was similar with both mapping methods, suggesting that the 2 quantitative mapping procedures can reveal the size of the array of the functional connections that are, at least, ~0.56 mm in V1.

Local Versus Global Mapping

This study is the first to use large-scale quantitative mapping methods to evaluate the cortical reorganization in V1 after a monocular retinal lesion. We used microelectrode array recordings together with 2 quantitative mapping methods to investigate the reorganization evoked by this lesion. The use of quantitative mapping methods associated with the repetitive recordings of the neuronal clusters along the same cell columns provided an important reduction in bias and increased the precision of our results relative to previous studies. The repeated RF mapping allowed the use of the RF scatter to evaluate the topographic reorganization. Additionally, this is the first study to use the quantitative global mapping method to show functional RFs inside the LPZ.

Before retinal lesioning, the RFs mapped with both methods, through both eyes, were binocularly matched. There was no significant difference in the RF area or in the scatter between the RFs mapped through each eye, both inside and outside the expected LPZ.

After retinal lesioning, for each mapping method, we saw changes in the RF locations obtained through the lesioned eye, while for the control eye the topography remained unchanged. For example, active cells were observed up to 0.85 mm inside the LPZ. These results are similar to those described by Gilbert and Wiesel (1992) and Darian-Smith and Gilbert (1995), who found a restricted reorganization in the LPZ (~0.5 mm) and a small RF displacement (1°) in V1 of anesthetized adult cats and macaque monkeys. Smirnakis et al. (2005) also observed a restricted reorganization in the LPZ (1 mm) of adult macaque monkeys using functional magnetic resonance imaging (fMRI). In contrast to our study, they found no reorganization with electrophysiological recordings. Heinen and Skavenski (1991) described the larger range of

LPZ reorganization in V1, immediately after retinal lesioning in awake adult macaque monkeys (1–2 mm). The difference in the results obtained by Heinen and Skavenski (1991) and our study might be explained by the use of awake versus anaesthetized preparations, and the foveal location of their lesion. Differences in anesthesia could also explain why Smirnakis et al. (2005), who used thiopental, did not find any electrophysiological responses inside the LPZ. Bourne and Rosa (2003) observed that thiopental tends to depress the electrophysiological recordings for many hours thereafter. However, Chino et al. (1992) and Calford et al. (1999), using anesthetized adult cats, observed a larger reorganization in V1 (~3 mm) and a larger RF displacement (~5 mm), while Murakami et al. (1997) observed no reorganization in the LPZ in V1 of adult awake macaque monkeys. In the present study, the local mapping data show a restricted reorganization similar to that observed in most previous studies in which anesthetized monkeys were also used. The differences in the results could also be due to the different eccentricities of the lesions, as there is some evidences that the response properties of cells in central and peripheral V1 may be slightly different (Battaglini et al. 1993; Yu et al. 2010). An early report has also shown that the representation of the periphery may have a lesser capacity to show the topographic reorganization, particularly short-term reorganization (Rosa et al. 1995). The different results could also be related to the different species and to the different qualitative mapping methods used in earlier studies.

In contrast to our results with the local mapping method, the global mapping method revealed evidence of more extensive reorganization—up to 1.87 mm. Most RFs were also located inside the LPZ, although displaced, likely reflecting the contribution of an active mechanism for interpolation of contours (Fiorani et al. 1992). In addition, all RFs located both inside and outside the LPZ presented a larger area and scatter than the RFs mapped through the control eye. Using a long moving bar as a stimulus, Fiorani et al. (1992) observed RFs inside the optic disc representation in V1 of adult monkeys. They also found a larger scatter and RF size for the optic disc mapping. In contrast to our results, they observed that the RFs were well-matched binocularly. They suggested that this interpolation process is mediated by convergent radial long-range horizontal connections and that the RF sizes reflected the degree of contribution of these connections. In our study, we also found RFs inside the optic disc representation with an overall small scatter. The same mechanism proposed by Fiorani et al. (1992) could be responsible for the RFs mapped in the LPZ. The rapid reorganization observed after retinal lesioning could be due to the unmasking of the pre-existing subthreshold connections in the surround of the RF (Chino et al. 1992; Gilbert and Wiesel 1992; Darian-Smith and Gilbert 1995; Calford et al. 1999). This unmasking process occurs quickly, as described in previous studies, that used masking of RFs (Fiorani et al. 1992; Pettet and Gilbert 1992; Volchan and Gilbert 1995; Eysel et al. 1998). The unmasked connections lead to an RF expansion. This RF expansion could explain the increase in RF scatter, which results from a direct relationship between the RF area and RF scatter as described by Hubel and Wiesel (1968). The same unmasking mechanism could also be responsible for the increase in the RF area and RF scatter observed outside the LPZ, where neighboring geniculo-striate axon collateral arbors could exert some inhibition in the intracortical connections before retinal lesioning. However, comparing the ratio in the RF scatter between the lesioned and control eyes, we saw a 5-fold increase inside the LPZ against 1.5-fold outside. Therefore, the effect of the retinal lesion outside the LPZ, although significant, was much weaker than inside.

Although a more coherent topography can be seen in LPZ using the global mapping method as opposed to the local mapping method, the global method shows a larger scatter for the lesioned eye than was previously observed for the optic disc (Fiorani et al. 1992). One possible explanation is the difference in time courses and development period following an acute retinal lesion and, versus that of the organogenesis of the visual system with the development of the optic disc.

With regard to the neuronal responses measured by the S/N ratio, most neurons inside the LPZ showed a dominance of the ipsilateral eye before lesioning. This can be explained by the presence, in the control eye, of the optic disc representation inside or around the electrode array and also by a random imbalance in the sampling of ocular dominance columns. As observed by Rosa et al. (1992), in *Cebus* monkeys, these columns are 300–400 μm thick, and our electrode arrays had 1400 or 700 μm spacing between electrodes. After retinal lesioning, many neuronal clusters inside the LPZ became nonresponsive to our mapping methods. Although some showed driven responses, they were weaker to the stimulation of the lesioned eye than of the control eye. This may reflect the loss of their main inputs and the unmasking of the subthreshold connections. In addition, we observed the same effect outside the LPZ with global mapping only. This result can be explained by a reduction in inhibitory influences from inside the LPZ upon neurons just outside it. As this result was only observed with the global method, it reinforces the suggestion that the alterations are dependent of the surrounding region of the RF. It is possible, however, that with a longer post-lesion recovery time, these connections could be use reinforced and that their responses, as well as the area of the RFs, would then return to their normal level (Darian-Smith and Gilbert 1995; Schmid et al. 1995; Giannikopoulos and Eysel 2006).

Possible Mechanisms Involved in the LPZ Reorganization

The short timeframe observed between the lesioning and the functional topographic changes points to an unmasking process that reveals pre-existing synaptic intracortical connections, as has been proposed by many previous studies (Heinen and Skavenski 1991; Chino et al. 1992; Gilbert and Wiesel 1992; Darian-Smith and Gilbert 1995; Schmid et al. 1995; Calford et al. 1999, 2000, 2003; Giannikopoulos and Eysel 2006). This unmasking process could be mediated by a decrease of the gamma amino butyric acid (GABA) levels in V1, as it has been observed following a retinal lesion (Arckens et al. 2000; Botelho et al. 2006). No studies have looked for acute GABA alterations in V1 of adult mammals, but in the sensorimotor cortex of adult humans, GABA levels decrease 30 min after hand deafferentation (Levy et al. 2002). In a recent study, Keck et al. (2011) showed that removal of visual input in adult mouse correlates with a rapid and lasting reduction in the number of inhibitory cell spines and

boutons. It is very unlikely that new projections could be established in such a short time because establishing new projections require gene expression and protein synthesis (Krahe et al. 2005). However, Yamahachi et al. (2009) showed an increase in axon density within the LPZ immediately after lesioning. Axon collateral sprout and synaptic buttons proliferate from the outset of the lesioning. In a post-lesion, long-recovery time, anatomical changes could occur that would promote a stabilization of the recovered LPZ (Darian-Smith and Gilbert 1994). More recent studies have demonstrated an upregulation of genes involved in creating the axonal cytosketon (Chen et al. 2010) and changes in the expression of immediate early genes (Hu et al. 2009) inside the LPZ and peri-LPZ.

Among all the possible connections inducing this reorganization, the V1 horizontal connections seem to be the more plausible candidates (Chino 1995; Calford et al. 2003), because they reach long distances (up to ~8 mm) and they connect cells with the same properties (Gilbert et al. 1996). The horizontal connections could also explain why these "recovered" neurons maintain their original properties (Chino et al. 1992, 1995; Chino 1995; Calford et al. 2000; Matsuura et al. 2002). Obata et al. (1999) found changes in molecular factors that could be involved in the reorganization process through the reinforcement of existing connections. These changes were stronger in the supragranular layers where the horizontal connections are more concentrated (Darian-Smith and Gilbert 1994). Young et al. (2007) showed that the convergent shifts of the RFs after retinal damage seem to require increased neuronal gain and are dependent on the temporal order of pre- and postsynaptic action potentials. The collateral arbors from neighboring geniculostriate axons of the neurons inside the LPZ could also be responsible for a very restricted reorganization in the LPZ (up to 0.6 mm, Blasdel and Fitzpatrick 1984). Although the horizontal connections could explain the post-lesional cortical reorganization, we cannot rule out the participation of the massive, and highly divergent, feedback cortical connections from higher hierarchical areas upon V1 (Gattass et al. 2005; Angelucci and Bressloff 2006).

Monocular Versus Binocular Retinal Lesion

As most neurons in V1 respond to the stimulation of both eyes, an important issue is whether binocular lesions are necessary to produce the visuotopic reorganization. Some previous works showed reorganization after monocular lesion only when the other eye is removed (Kaas et al. 1990; Chino et al. 1992). However, Schmid et al. (1996) showed that the visuotopic reorganization after monocular lesion is not altered after photocoagulation of the optic disc of the other eye. This paper is the first to show unambiguously that reorganization following monocular lesions is possible, using quantitative methods. Our data demonstrate that even in the presence of competing normal (control) eye inputs, a restricted reorganization in the LPZ in V1 is present immediately after retinal lesioning. The absence of control eye inputs can facilitate this reorganization, as we observed in animal M4 where the optic disc of the control eye was partially superimposed on the retinal lesion. In the case of the animal M4, we observed a larger functional reorganization in the optic disc binocular silent zone (1.87 mm) than in the monocular zone outside the optic disc (1.15 mm).

Consequences for Visual Perception

Another important question is how this topographic reorganization could influence visual perception. The theoretical purpose of the post-traumatic reorganization is the attempt to recover function. However, these recovered abnormal binocular RF disparities could promote an amblyopic vision or at least abnormal stereoscopic (3D) perceptions. In the optic disc representation in V1, the RFs are somewhat binocularly matched, which seems to prevent abnormal perceptions in this region (Fiorani et al. 1992, 2001). Perhaps under binocular vision, the connections from the normal eye inhibit the response to the stimulation of the lesioned eye (binocular rivalry), thereby avoiding abnormal binocular disparities. Matsuura et al. (2002) showed that the binocular interaction between the lesioned and the normal eyes was inhibitory to RFs with 3° of binocular disparity. Schmid et al. (1996) also observed that although the LPZ underwent reorganization in V1, the responses of the cells to the stimulation of the lesioned eye were inhibited for 10 s by the synaptic connections of the normal eye. Cohen et al. (2003) suggest that in humans, there is an inhibitory function of the normal eye in the filling-in process of the lesioned eye, but with homotopical binocular retinal lesioning, the filling-in process is facilitated. Nevertheless, under a monocular view, abnormal RF topography will also lead to visual distortion. Using the global mapping method, we found that the topography was closer to normal than it was using the local mapping method. The precision of the global mapping can be explained by the more natural characteristics of the stimulus, where the coherence of position, orientation, direction, and speed are processed together. Additionally, both mapping methods show the same median CRRF scatter (and distribution) inside the LPZ (0.56 mm), and although small, it is more than 4 times the scatter seen in the unlesioned retina (0.12 mm). Despite the differences in the topography seen with these 2 methods and the distance inside the LPZ in which we found responsive neurons (up to 1.86 mm), the CRRF scatter of 0.56 mm for the LPZ must represent an average functional limit for changes in the visual field representation. Although recording repetitively, we produced only a very small sample of the V1 information required to render visual perception.

For further study, additional quantitative mapping and more standardized methods should be employed to answer the question of whether there is reorganization of the entire LPZ after monocular or binocular retinal lesioning, as well as to investigate the timeframe required for the reorganization and the visual perception consequences of retinal lesions.

Funding

This research was supported by grants from the following institutions: CAPES, CNPq, FAPERJ, PRONEX, and FINEP. Funding to pay the Open Access publication charges for this article was provided by CNPq (Proc. 55.0003/2011-8).

Notes

The authors are grateful to Dr Sergio Neuenschwander for his generous contribution of the Spass program; Drs Aglai Souza and Andreas Frick for comments on the manuscript; Edil Saturato, Liliane Heringer, Paulo Coutinho, and Thereza Monteiro for technical support; Drs Andreia Zin, Eduardo Damasceno, and Renato David for helping with

the retinal lesioning; and OPTO S.A. (São Paulo, Brazil), which kindly loaned the laser used for the retinal lesioning procedure. *Conflict of Interest*: None declared.

References

Airaksinen PJ, Tuulonen A. 1993. Retinal nerve fiber layer evaluation. In: Varma R, editor. The optic nerve in glaucoma. Philadelphia (PA): JB Lippincott Company. p. 277–289.

Angelucci A, Bressloff PC. 2006. Contribution of feedforward, lateral and feedback connections to the classical receptive field center and extra-classical receptive field surround of primate V1 neurons. Prog Brain Res. 154:93–120.

Angelucci A, Levitt JB, Walton EJ, Hupe JM, Bullier J, Lund JS. 2002. Circuits for local and global signal integration in primary visual cortex. J Neurosci. 22:8633–8646.

Arckens L, Schweigart G, Qu Y, Wouters G, Pow DV, Vandesande F, Eysel UT, Orban GA. 2000. Cooperative changes in GABA, glutamate and activity levels: the missing link in cortical plasticity. Eur J Neurosci. 12:4222–4232.

Azzi JCB. 2004. O mapa do cortex visual primario (V1) é "visuotópico" e não "retinotópico": visuotopia do ponto cego em V1 de primatas (Cebus apella) [Federal University of Rio de Janeiro PhD thesis]. Rio de Janeiro (Brazil): Federal University of Rio de Janeiro Publication. (p. 129).

Battaglini PP, Galletti C, Fattori P. 1993. Functional properties of neurons in area V1 of awake macaque monkeys: peripheral versus central visual field representation. Arch Ital Biol. 131:303–315.

Blasdel GG, Fitzpatrick D. 1984. Physiological organization of layer 4 in macaque striate cortex. J Neurosci. 4:880–895.

Botelho EP, Ceriatti C, Soares JGM, Gattass R, Fiorani M. 2007. Limited receptive field reorganization in V1 of adult primate immediately after restricted monocular retinal lesion. Soc Neurosci. Online Program No. 279.15 [Abstract].

Botelho EP, Soares JGM, Pereira SS, Fiorani M, Gattass R. 2006. Distribution of calbindin-28kD and parvalbumin in V1 in normal adult Cebus apella monkeys and in monkeys with retinal lesions. Brain Res. 1117:1–11.

Bourne JA, Rosa MG. 2003. Preparation for the in vivo recording of neuronal responses in the visual cortex of anaesthetised marmosets (Callithrix jacchus). Brain Res Brain Res Protoc. 11:168–177.

Calford MB, Schmid LM, Rosa MG. 1999. Monocular focal retinal lesions induce short-term topographic plasticity in adult cat visual cortex. Proc Biol Sci. 266:499–507.

Calford MB, Wang C, Taglianetti V, Waleszczyk WJ, Burke W, Dreher B. 2000. Plasticity in adult cat visual cortex (area 17) following circumscribed monocular lesions of all retinal layers. J Physiol. 524:587–602.

Calford MB, Wright LL, Metha AB, Taglianetti V. 2003. Topographic plasticity in primary visual cortex is mediated by local corticocortical connections. J Neurosci. 23:6434–6442.

Chen J, Yamahachi H, Gilbert CD. 2010. Experience-dependent gene expression in adult visual cortex. Cereb Cortex. 20:650–660.

Chino YM. 1995. Adult plasticity in the visual system. Can J Physiol Pharmacol. 73:1323–1338.

Chino YM, Kaas JH, Smith EL, III, Langston AL, Cheng H. 1992. Rapid reorganization of cortical maps in adult cats following restricted deafferentation in retina. Vision Res. 32:789–796.

Chino YM, Smith EL, III, Kaas JH, Sasaki Y, Cheng H. 1995. Receptive-field properties of deafferentated visual cortical neurons after topographic map reorganization in adult cats. J Neurosci. 15:2417–2433.

Cohen SY, Lamarque F, Saucet JC, Provent P, Langram C, LeGargasson JF. 2003. Filling-in phenomenon in patients with age-related macular degeneration: differences regarding uni- or bilaterality of central scotoma. Graefes Arch Clin Exp Ophthalmol. 241:785–791.

Darian-Smith C, Gilbert CD. 1994. Axonal sprouting accompanies functional reorganization in adult cat striate cortex. Nature. 368:737–740.

Darian-Smith C, Gilbert CD. 1995. Topographic reorganization in the striate cortex of the adult cat and monkey is cortically mediated. J Neurosci. 15:1631–1647.

Eysel UT, Eyding D, Schweigart G. 1998. Repetitive optical stimulation elicits fast receptive field changes in mature visual cortex. Neuroreport. 9:949–954.

Fiorani M, Azzi JC, Gattass R. 2001. Primate V1 has a visuotopic rather than a retinotopic organization: the topographic organization of the blind spot (BS) in V1. Soc Neurosci. Online Program No. 619.46 [Abstract].

Fiorani M, Jr, Rosa MG, Gattass R, Rocha-Miranda CE. 1992. Dynamic surrounds of receptive fields in primate striate cortex: a physiological basis for perceptual completion? Proc Natl Acad Sci USA. 89:8547–8551.

Fiorani M, Oliveira L, Volchan E, Gattass R, Rocha-Miranda CE, Pessoa L. 2003. Completion through a permanent scotoma: fast interpolation across the blind spot and the processing of occlusion. In: Pessoa LA, de Weerd P, editors. Filling-in: from perceptual completion to cortical reorganization. New York (NY): Oxford University Press. p. 187–206.

Freese CH, Oppenheimer JH. 1981. The capuchin monkeys, genus Cebus. In: Coimbra-Filho AF, Mittermeier RA, editors. Ecology and behavior of neotropical primates. Rio de Janeiro (Brazil): Academia Brasileira de Ciências. p. 331–390.

Gattass R, Nascimento-Silva S, Soares JG, Lima B, Jansen AK, Diogo AC, Farias MF, Botelho MM, Mariani OS, Azzi J *et al*. 2005. Cortical visual areas in monkeys: location, topography, connections, columns, plasticity and cortical dynamics. Philos Trans R Soc Lond B Biol Sci. 360:709–731.

Gattass R, Sousa AP, Rosa MG. 1987. Visual topography of V1 in the Cebus monkey. J Comp Neurol. 259:529–548.

Giannikopoulos DV, Eysel UT. 2006. Dynamics and specificity of cortical map reorganization after retinal lesions. Proc Natl Acad Sci USA. 103:10805–10810.

Gilbert CD, Das A, Ito M, Kapadia M, Westheimer G. 1996. Spatial integration and cortical dynamics. Proc Natl Acad Sci USA. 93:615–622.

Gilbert CD, Wiesel TN. 1992. Receptive field dynamics in adult primary visual cortex. Nature. 356:150–152.

Heinen SJ, Skavenski AA. 1991. Recovery of visual responses in foveal V1 neurons following bilateral foveal lesions in adult monkey. Exp Brain Res. 83:670–674.

Hu TT, Laeremans A, Eysel UT, Cnops L, Arckens L. 2009. Analysis of c-fos and zif268 expression reveals time-dependent changes in activity inside and outside the lesion projection zone in adult cat area 17 after retinal lesions. Cereb Cortex. 19:2982–2992.

Hubel DH, Wiesel TN. 1968. Receptive fields and functional architecture of monkey striate cortex. J Physiol. 195:215–243.

Hubel DH, Wiesel TN. 1974. Uniformity of monkey striate cortex: a parallel relationship between field size, scatter, and magnification factor. J Comp Neurol. 158:295–305.

Kaas JH, Krubitzer LA, Chino YM, Langston AL, Polley EH, Blair N. 1990. Reorganization of retinotopic cortical maps in adult mammals after lesions of the retina. Science. 248:229–231.

Keck T, Scheuss V, Jacobsen RI, Wierenga CJ, Eysel UT, Bonhoeffer T, Hübener M. 2011. Loss of sensory input causes rapid structural changes of inhibitory neurons in adult mouse visual cortex. Neuron. 71:869–882.

Komatsu H, Kinoshita M, Murakami I. 2000. Neural responses in the retinotopic representation of the blind spot in the macaque V1 to stimuli for perceptual filling-in. J Neurosci. 20:9310–9319.

Krahe TE, Medina AE, de Bittencourt-Navarrete RE, Colello RJ, Ramoa AS. 2005. Protein synthesis-independent plasticity mediates rapid and precise recovery of deprived eye responses. Neuron. 48:329–343.

Le Gros Clark WE. 1959. The antecedents of man. Edinburgh (UK): Edinburgh University Press.

Levy ML, Ziemann U, Chen R, Cohen LG. 2002. Rapid modulation of GABA in sensorimotor cortex induced by acute deafferentation. Ann Neurol. 52:755–761.

Matsuura K, Zhang B, Mori T, Smith EL, III, Kaas JH, Chino Y. 2002. Topographic map reorganization in cat area 17 after early monocular retinal lesions. Vis Neurosci. 19:85–96.

McIlwain JL. 1976. Large receptive fields and spatial transformations in the visual system. Int Rev Physiol. 10:223–249.
Murakami I, Komatsu H, Kinoshita M. 1997. Perceptual filling-in at the scotoma following a monocular retinal lesion in the monkey. Vis Neurosci. 14:89–101.
Obata S, Obata J, Das A, Gilbert CD. 1999. Molecular correlates of topographic reorganization in primary visual cortex following retinal lesions. Cereb Cortex. 9:238–248.
Pettet MW, Gilbert CD. 1992. Dynamic changes in receptive-field size in cat primary visual cortex. Proc Natl Acad Sci USA. 89:8366–8370.
Polimeni JR, Balasubramanian M, Schwartz EL. 2006. Multi-area visuotopic map complexes in macaque striate and extra-striate cortex. Vision Res. 46:3336–3359.
Rosa MG, Gattass R, Fiorani M, Jr, Soares JG. 1992. Laminar, columnar and topographic aspects of ocular dominance in the primary visual cortex of Cebus monkeys. Exp Brain Res. 88:249–264.
Rosa MG, Schmid LM, Calford MB. 1995. Responsiveness of cat area 17 after monocular inactivation: limitation of topographic plasticity in adult cortex. J Physiol. 482:589–608.
Rosa MG, Soares JG, Fiorani M, Jr, Gattass R. 1993. Cortical afferents of visual area MT in the Cebus monkey: possible homologies between new and old world monkeys. Vis Neurosci. 10:827–855.
Schmid LM, Rosa MG, Calford MB. 1995. Retinal detachment induces massive immediate reorganization in visual cortex. Neuroreport. 6:1349–1353.
Schmid LM, Rosa MG, Calford MB, Ambler JS. 1996. Visuotopic reorganization in the primary visual cortex of adult cats following monocular and binocular retinal lesions. Cereb Cortex. 6:388–405.
Silverman MS, Tootell RB. 1987. Modified technique for cytochrome oxidase histochemistry: increased staining intensity and compatibility with 2-deoxyglucose autoradiography. J Neurosci Methods. 19:1–10.
Smirnakis SM, Brewer AA, Schmid MC, Tolias AS, Schüz A, Augath M, Inhoffen W, Wandell BA, Logothetis NK. 2005. Lack of long-term cortical reorganization after macaque retinal lesions. Nature. 435:300–307.
Soares JG, Diogo AC, Fiorani M, Souza AP, Gattass R. 2004. Effects of inactivation of the lateral pulvinar on response properties of second visual area cells in Cebus monkeys. Clin Exp Pharmacol Physiol. 31:580–590.
Volchan E, Gilbert CD. 1995. Interocular transfer of receptive field expansion in cat visual cortex. Vision Res. 35:1–6.
Waleszczyk WJ, Wang C, Young JM, Burke W, Calford MB, Dreher B. 2003. Laminar differences in plasticity in area 17 following retinal lesions in kittens or adult cat. Eur J Neurosci. 17:2351–2368.
Yamahachi H, Marik SA, McManus JN, Denk W, Gilbert CD. 2009. Rapid axonal sprouting and pruning accompany functional reorganization in primary visual cortex. Neuron. 64: 719–729.
Young JM, Waleszczyk WJ, Wang C, Calford MB, Dreher B, Obermayer K. 2007. Cortical reorganization consistent with spike timing-but not correlation-dependent plasticity. Nat Neurosci. 10:887–895.
Yu HH, Verma R, Yang Y, Tibballs HA, Lui LL, Reser DH, Rosa MG. 2010. Spatial and temporal frequency tuning in striate cortex: functional uniformity and specializations related to receptive field eccentricity. Eur J Neurosci. 31:1043–1062.